Chem Soc Rev

Upconverting nanoparticles: a versatile platform for wide-field two-photon microscopy and multi-modal in vivo imaging

Journal:	*Chemical Society Reviews*
Manuscript ID:	CS-REV-05-2014-000173.R1
Article Type:	Tutorial Review
Date Submitted by the Author:	04-Jul-2014
Complete List of Authors:	Park, Yong Il; Seoul National University, School of Chemical and Biological Engineering Lee, Kang Taek; Gwangju Institute of Science and Technology (GIST), Department of Chemistry Suh, Yung Doug; Korea Research Institute of Chemical Technology, Research Center for Convergence Nanotechnology Hyeon, Taeghwan; Seoul National University, School of Chemical and Biological Engineering

Upconverting nanoparticles: a versatile platform for wide-field two-photon microscopy and multi-modal *in vivo* imaging

Yong Il Park,[abf] *Kang Taek Lee,*[cf] *Yung Doug Suh**[de] *and Taeghwan Hyeon**[ab]

[a] *Center for Nanoparticle Research, Institute for Basic Science (IBS), Seoul 151-742, Korea*

[b] *School of Chemical and Biological Engineering, Seoul National University, Seoul 151-742, Korea*

E-mail: thyeon@snu.ac.kr

[c] *Department of Chemistry, Gwangju Institute of Science and Technology (GIST), Gwangju 500-712, Korea*

[d] *Laboratory for Advanced Molecular Probing (LAMP), Research Center for Convergence Nanotechnology, Korea Research Institute of Chemical Technology, Daejeon 305-600, Korea*

E-mail: ydsuh@krict.re.kr

[e] *School of Chemical Engineering, Sungkyunkwan University, Suwon 440-746, Korea*

[f] *These authors contributed equally to this work.*

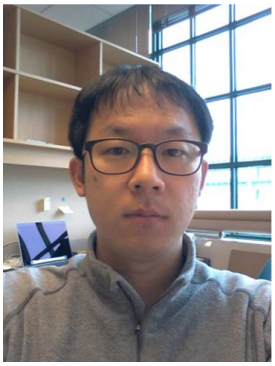

Yong Il Park received his B.S. (2005) and Ph.D. (2011) from Chemical and Biological Engineering of Seoul National University under the supervision of Prof. Taeghwan Hyeon. During his doctorate period, he worked on the development of lanthanide-doped upconverting nanoparticles and their biomedical application. He is currently a postdoctoral researcher working with Prof. Hakho Lee and Prof. Ralph Weissleder at Harvard Medical School/Massachusetts General Hospital.

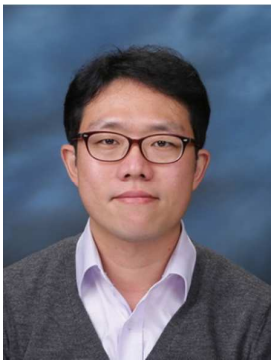

Kang Taek Lee received his B.S. (1996), M.S. (1998), and Ph.D. (2003) (supervisor: Prof. Seong Keun Kim) in the Department of Chemistry of Seoul National University. He worked as a postdoctoral researcher at Harvard University (supervisor: Prof. X. Sunney Xie) and the University of Chicago (supervisor: Prof. Norbert F. Scherer) until he became a senior researcher at Korea Research Institute of Chemical Technology (KRICT) in 2007. In March 2013, he joined the faculty of the Department of Chemistry at Gwangju Institute of Science and Technology (GIST). His new research group is focusing on developing the optical imaging methods, particularly employing multifunctional nanoparticle probes to directly monitor the dynamics in live cells.

Dr. Yung Doug Suh studied at Seoul National University for his B.S. (1991), M.S. (1993), and Ph.D. (1999) under the guidance of Prof. Seong Keun Kim in Chemistry Department, Dr. Dongho Kim in Korea Research Inst. of Standards and Science (KRISS), and Prof. Young Kuk in Physics researching gas phase molecular reaction dynamics, laser spectroscopies, and surface physics with

UHV-STM, respectively. After finishing the postdoctoral research in ETH Zurich with Prof. Renato Zenobi (1999–2000), he worked at the Pacific Northwest National Laboratory (PNNL), USA (2001–2002). He accepted his current position in 2003, to form his own research group: Laboratory for Advanced Molecular Probing (LAMP) at the Korea Research Institute of Chemical Technology (KRICT) in Daejeon, Korea.

Taeghwan Hyeon received his B. S. (1987) and M. S. (1989) from Chemistry in Seoul National University. He obtained his Ph. D. (1996) from Chemistry in University of Illinois at Urbana-Champaign. Since he joined the faculty of the School of Chemical and Biological Engineering of Seoul National University in September 1997, he has focused on the synthesis and applications of uniform-sized nanocrystals and nanoporous materials. He is a Director of Center for Nanoparticle Research in the Institute for Basic Science (IBS). He is currently serving as an Associate Editor of *J. Am. Chem. Soc.*, and editorial advisory board members of *Adv. Mater., Nanoscale, Nano Today*, and *Small*.

Table of Contents

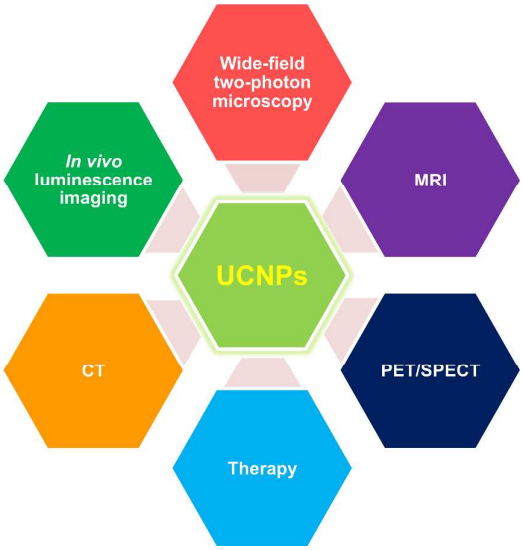

Upconverting nanoparticles (UCNPs) enable the establishment of a novel UCNP-based platform for wide-field two-photon microscopy and multimodal *in vivo* imaging.

Abstract. Lanthanide-doped upconverting nanoparticles (UCNPs) have recently attracted enormous attention in the field of biological imaging owing to their unique optical properties: 1) efficient upconversion photoluminescence, which is intense enough to be detected at the single-particle level with a (nonscanning) wide-field microscope setup equipped with a continuous wave (CW) near-infrared (NIR) laser (980 nm), and 2) resistance to photoblinking and photobleaching. Moreover, the use of NIR excitation minimizes adverse photoinduced effects such as cellular photodamage and the autofluorescence background. Finally, the cytotoxicity of UCNPs is much lower than that of other nanoparticle systems. All these advantages can be exploited simultaneously without any conflicts, which enable the establishment of a novel UCNP-based platform for wide-field two-photon microscopy. UCNPs are also useful for multimodal *in vivo* imaging because simple variations in the composition of the lattice atoms and dopant ions integrated into the particles can be easily implemented, yielding various distinct biomedical activities relevant to magnetic resonance imaging (MRI), computed tomography (CT), and positron emission tomography (PET). Those multiple functions embedded in a single type of UCNPs play a crucial role in precise disease diagnosis. The application of UCNPs is extended to therapeutic fields such as photodynamic and photothermal cancer therapies through advanced surface conjugation schemes.

Key learning points

(1) Lanthanide-ion-doped upconverting nanoparticles (UCNPs) exhibit 1) anti-Stokes photoluminescence in the visible spectral range upon absorption of near-infrared (NIR) photons through an optical upconversion process, 2) extreme photostability (no photoblinking and no photobleaching), and 3) low cytotoxicity.

(2) The use of NIR excitation completely suppresses cellular autofluorescence and photoinduced damage to cells.

(3) UCNPs provide a novel versatile platform for wide-field two-photon imaging that overcomes the drawbacks of conventional two-photon microscopy while maintaining its advantages.

(4) The UCNP library with various lanthanide elements supports multiple imaging modalities, including luminescence imaging, magnetic resonance imaging, positron emission tomography, and computed tomography.

(5) UCNPs designed for medical purposes will provide enhanced diagnostic and therapeutic efficacy.

1. Introduction

Anti-Stokes emitting molecules and materials have attracted great attention recently as next-generation luminescent materials in the fields of energy, biology, and medicine. Their emission wavelength is shorter than that of the excitation light, where the relevant photophysical processes include the upconversion process, second-harmonic generation, and two-photon absorption. Among them, the upconversion process is the most efficient because it involves stable intermediate states. Since their discovery in 1966, upconverting phosphors have been synthesized by doping d and f elements into hosts.[1,2] In particular, lanthanide-doped upconverting materials have been studied most intensively because of their bright upconversion luminescence at room temperature, and they have been used for various applications such as lasers, infrared quantum counters, and displays.[1,2] Most notably, there have been tremendous efforts to synthesize nanosized "upconverting particles" and apply them to biological imaging, early-stage diagnoses, and therapeutics in past years, in which their unique optical properties, namely, the absorption of near-infrared (NIR) photons and the emission of visible and ultraviolet (UV) photons are widely exploited.[3,4] Technological advances in nanomaterial synthesis and surface functionalization have prompted researchers to develop upconverting nanoparticles (UCNPs) featuring a homogeneous chemical composition, a narrow size distribution, and biological functions.[5–7]

The photophysical pathway associated with upconversion photoluminescence is relatively well understood. The widely accepted energy level diagram of the representative UCNPs $NaYF_4$:Yb^{3+},Er^{3+} and their photoluminescence spectra for the α type (cubic phase) and β type (hexagonal phase) are shown in Figure 1.[8] A Yb^{3+} in the UCNPs absorbs a 980-nm photon to the $^2F_{5/2}$ state and transfers its excitation energy to the $^4I_{11/2}$ state of a neighboring Er^{3+}. The energies of those two states are very close, which allows the energy to be transferred efficiently. Subsequently, an additional energy transfer occurs from another Yb^{3+} to the Er^{3+},

resulting in further excitation to a higher level of Er^{3+} ($^4F_{7/2}$). After fast nonradiative relaxation to one of the three states that are slightly lower in energy ($^2H_{11/2}$, $^4S_{3/2}$, or $^4F_{9/2}$), the doubly exited Er^{3+} emits one photon (*ca.* 525, 550, or 660 nm, respectively) whose energy is slightly less than that of two 980-nm photons. For the red emission around 660 nm, a possible alternative photophysical mechanism has been suggested in which nonradiative relaxation occurs from the intermediate excited state of Er^{3+} ($^4I_{11/2}$) to a lower-energy state ($^4I_{13/2}$) immediately after the first energy transfer, instead of the above-mentioned possibility occurring between $^4F_{7/2}$ and $^4F_{9/2}$ (Figure 1a).[9,10] The emission efficiency of UCNPs also depends on the crystal structure of the host materials. Hexagonal phase UCNPs usually exhibit about 10 times more intense green emission than cubic phase ones, which is originated from the interaction of lanthanide ions in the two different lattice structures.[2] Cubic phase sodium rare earth (RE) fluoride ($NaREF_4$) has fluorite structure with one type of high-symmetry cation sites that are randomly occupied by Na^+ and RE^{3+} ions (Figure 1d). On the contrary, hexagonal phase $NaREF_4$ has two types of low-symmetry cation sites that are selectively occupied by Na^+ and RE^{3+} ions (Figure 1e).[11] Thus, the UCNPs with hexagonal structure reduce unnecessary cross-relaxation among the doped-lanthanide ions, resulting in more efficient upconversion luminescence than the cubic ones.

The upconversion photoluminescence of UCNPs is not only an exotic and interesting photophysical phenomenon but also has a great deal of potential for biological imaging. The upconversion process, which converts NIR photons to visible photons, improves cellular imaging techniques by providing a variety of benefits resulting from the extreme photostability of UCNPs and the use of a NIR (980-nm) laser as the excitation light source.

It is interesting to compare the upconversion process to two-photon absorption, which is employed in conventional two-photon microscopy. They resemble each other in that the emitters (Er^{3+} in UCNPs in the former and dye molecules in the latter) are excited twice by

two quanta of energy. However, the first distinct feature of upconversion photoluminescence is that the excitation occurs in the sensitizer Yb^{3+} cations rather than in the emitter Er^{3+} cations themselves. This is because the absorption efficiency (extinction coefficient) of the electronic transition of Yb^{3+} is much higher than that of Er^{3+} at 980 nm.[12] The energy transfer occurring after absorption is responsible for the two-photon excitation of the emitter, Er^{3+}, whereas, in normal two-photon microscopy, the emitter (dye molecule) itself is excited directly. The second, and more important, difference is that the intermediate excited state of Er^{3+} is a real state with a long lifetime on the millisecond time scale,[1] whereas the lifetime of two-photon dye molecules is extremely short because the excitation involves a "virtual" intermediate state. In the latter case, two-photon absorption becomes feasible only when the photon flux is sufficiently high within a very short period of time. Therefore, ultrashort laser pulses from femtosecond laser systems are commonly used to excite the dye molecules. On the other hand, the long lifetime of the intermediate excited state of Er^{3+} prepared after the first energy transfer from Yb^{3+} guarantees sufficient time for the second energy transfer to occur. This fact indicates that only moderate excitation power is needed to excite UCNPs, and it has been shown that a small, inexpensive continuous wave (CW) diode laser (980 nm) is an adequate light source. As a result, it follows that the wide-field microscopy can easily be realized for UCNP imaging. In typical two-photon microscopy, one has to focus the femtosecond laser pulse tightly on the sample and acquire fluorescence signals by scanning the sample or the laser beam over the field of view. In such cases, as in conventional confocal microscopy, the data acquisition time is significantly long. However, in the wide-field imaging mode, two-dimensional images are projected onto the detector in each round of data acquisition; therefore, the imaging frame rate can routinely be set as high as 10–100 frames/s if the luminescence is sufficiently strong, which is the case with UCNPs.[13]

UCNPs are also useful for *in vivo* imaging, which is related to biomedical applications such as accurate diagnosis and efficient therapy in diagnosing and prescribing treatment for certain diseases. In serious diseases such as cancer and neuronal disorders, treatment is simpler and more effective if the condition is diagnosed early. For instance, the five-year survival rate of women diagnosed with ovarian cancer at stage I is 93%, whereas that of patients diagnosed at stage III is 30%.[14] To achieve accurate diagnosis, a variety of medical imaging techniques have been developed: magnetic resonance imaging (MRI), computed tomography (CT), and positron emission tomography (PET), to name a few. These imaging tools have diverse degrees of sensitivity, spatial resolution, and imaging depth. MRI provides anatomical details based on soft-tissue contrast and functional information, but its sensitivity is relatively low. PET provides high detection sensitivity with low spatial resolution. To compensate for the limits of each imaging technique, a number of studies have attempted to develop novel multimodal imaging probes. UCNPs were recently recognized as a suitable candidate because various lanthanide ion dopants with distinct properties and functions can be integrated into individual particles. In other words, UCNPs can be developed as useful multimodal imaging probes for optical imaging, MRI, CT, and PET. Fortunately, it is technically easy to dope multiple types of lanthanide ions together into a host matrix because they have similar atomic sizes and chemical properties.

In this tutorial, we focus on the versatility of UCNPs as a platform for both wide-field two-photon microscopy and multimodal *in vivo* imaging.

2. UCNP-based wide-field two-photon imaging

2.1 Nonscanning wide-field imaging of UCNPs

As mentioned in the introduction, one of the most important consequences of the two-photon upconversion processes in UCNPs is that UCNPs can be imaged by wide-field

microscopy, such as epi-fluorescence and total internal reflection fluorescence (TIRF) microscopy, without scanning the sample or using laser excitation as in confocal microscopy (Figure 2). Epi-fluorescence microscopy is characterized by the collimated illumination on the sample and the collection of two dimensional fluorescence images by two-dimensional detectors such as charge coupled device (CCD) cameras. In general, this technique is appropriate for imaging a certain plane (focal plane of the objective lens) inside cells. However, the illumination that passes through the entire sample generates a significant signal not only from the focal plane but also from the out-of-focus region. The out-of-focus signal acts as the background that smears the image and, therefore, lowers the image contrast. On the other hand, confocal microscopy overcomes this problem by focusing the illuminating light source and placing a pinhole in front of the photo-detector such as photomultiplier tube (PMT) and avalanche photodiode (APD). In this scheme, the out-of-focus signals do not pass the hole and are not detected by the detector. As a result, the fluorescence signal only from the focal point reaches the detector without significant contamination. However, the rate of image acquisition is limited (~10 frames/s) because they are constructed by sequentially attaching the point signals obtained while scanning the sample or the focus of light. The confocal microscopy might be the best choice to investigate the cellular structure that is fixed or evolving very slowly. But it is not an appropriate tool for imaging fast dynamics in cells. TIRF microscopy adopts the advantages of the above-mentioned two microscopic techniques in that only the thin layers of evanescent electromagnetic field is illuminated, which removes the background signal from the cell body, and at the same time, the detection of two dimensional image is achieved with wide-field imaging scheme. But again, it cannot image the deeper structure of cells. For UCNPs, it turns out that the epi-fluorescence microscopy approach is especially useful. In particular, Park *et al*. showed that even photoluminescence of a single UCNP (cubic phase, diameter of *ca.* 40 nm) could be imaged with wide-field epi-

fluorescence microscopy.[5] Subsequently, Nam *et al*. reported the first real-time single-particle tracking of a UCNP (hexagonal phase, diameter of *ca*. 30 nm) internalized in a living cell at a frame rate of 20 Hz (50-ms exposure time per frame).[13] In those studies, the wide-field epi-fluorescence imaging setup consisted of an inverted microscope, a NIR (980-nm) CW diode laser, an electron-multiplying charge-coupled device (EMCCD) camera, and the optical components in the excitation and detection pathways. The laser was introduced to the microscope and directed to the UCNP-containing sample after being reflected by a dichroic beam splitter. This dichroic beam splitter was designed to reflect the excitation laser (980 nm) toward the sample through the center of the objective and to transmit the photoluminescence in a shorter wavelength range. Such short-pass dichroic separation is obviously required because the UCNP photoluminescence lies in the visible spectral region with a huge anti-Stokes shift from the NIR excitation (980 nm). As in typical epi-fluorescence microscopy, the incident excitation laser beam is focused on the back focal point of the objective by a lens placed in front of the entrance port of the microscope. This ensures that the beam is collimated to dimensions of tens of micrometers (typically ca. 60 μm x 60 μm) when it reaches the focal plane, where the samples are supposed to be. The photoluminescence from the excited UCNPs is collected by the same objective and directed to and projected at the detector chip of the EMCCD. In the middle of this detection pathway, the photoluminescence signals pass the dichroic beam splitter, whereas strong stray light (980 nm) is either scattered from the sample and the optics in the objective or reflected at the cover glass–sample interface. The residual 980-nm photons are further filtered out by a short-pass or band-pass filter with a transmission wavelength window below 700 nm. The image might be subject to further magnification by placing a pair of lenses with different focal lengths at the correct positions between the microscope output port and the camera. This additional magnification is required to adjust the actual dimensions of the images, which determine the typical number

of cells within the field of view in cellular imaging experiments. Sometimes it might be necessary to separately acquire the images by monitoring two distinct channels, namely, the green and red bands of the UCNPs, and this can be achieved by placing another set consisting of a dichroic beam splitter and band-pass filters between the microscope output port and the camera. Each of the separate images is finally projected on half of the EMCCD chip, as in most single-molecule Förster resonance energy transfer (FRET) studies.[15]

Traditionally, confocal microscopy is preferred in cellular imaging when one needs to construct three-dimensional images of cells because of its ability to eliminate the out-of-focus background and the resultant image sectioning capability. With the NIR laser that excites UCNPs, however, no autofluorescence is observed from the cell bodies, as will be elaborated in the following section. Therefore, the out-of-focus background is very low, and the section images over the *z* axis are readily resolved simply by adjusting the focal plane of the objective. The "confocal-like" sectioning capability of wide-field imaging is one of the most attractive aspects of UCNP-based imaging. More recently, UCNPs were successfully imaged with TIRF microscopy.[16] TIRF imaging will obviously provide more clear information on the cell membrane dynamics adjacent to the cover glass, where the *ca.* 100-nm-thick evanescent electromagnetic field is generated.

2.2 Photostability of UCNPs

The photostability of fluorescent molecules or luminescent nanomaterials can be discussed according to two distinct characteristics: (1) how much the luminescence intensity fluctuates over the data acquisition time and (2) how long the luminescence persists under continuous irradiation.

Regarding the first point, photoblinking is of the most concern, especially in single-molecule or live cell imaging. It is a type of on-off fluctuation of the photoluminescence

observed even under continuous excitation. Semiconductor nanocrystals (quantum dots, QDs) are the most intensively studied systems with regard to photoblinking.[17,18] Although a number of mechanisms have been suggested, the exact mechanism is yet to be determined. Photoblinking limits the use of QDs as an imaging probe, especially in single-particle tracking studies, where continuous or uninterrupted photoluminescence is crucial. On the other hand, UCNPs have been known to exhibit no photoblinking at the single-particle level, as shown in Figure 3.[5,19] The photoluminescence intensity is preserved constantly without any dark period. This property of UCNPs, combined with the fact that they are bright enough to be detected at the single-particle level, enables continuous imaging with millisecond or microsecond temporal resolution.[13] It is not clear yet whether photoblinking does not occur in individual Er^{3+}-Yb^{3+} upconversion units. However, one may simply note that, even if it does, the upconversion processes occurring in a particle among numerous randomly positioned Er^{3+} and Yb^{3+} ions would statistically produce constant photoluminescence.[19]

The second point to consider regarding photostability is a phenomenon called photobleaching. Most luminescent objects irreversibly lose their capability to emit photons after a finite period of excitation owing to chemical degradation to nonfluorescent states, occurring presumably in the excited state. For example, single organic dye molecules and fluorescent proteins are bleached within seconds or minutes when they are excited by a laser or any other light source with the typical power density for single-molecule imaging. Photobleaching obviously limits the time window for observation or imaging because dynamics with a duration longer than the typical lifetime of the probes cannot be fully measured, so only short temporal fragments of information are obtained. Inorganic nanoparticle systems generally exhibit much less photobleaching than organic dyes.[15] In particular, with single-particle imaging, it has been demonstrated that the luminescence of UCNPs is extremely resistant to photobleaching even under hours of continuous

excitation.[5,19] This remarkable characteristic behavior indicates that the sensitizer-emitter dopant cations do not undergo chemical degradation as a result of repeated excitation-photoluminescence cycles.[3] Moreover, the robust $NaYF_4$ crystal systems are likely to protect the dopant cations. This might be one of the greatest advantages of UCNPs for biological imaging.[7] As a result, long-term (6 h) continuous live cell imaging is possible using UCNPs, providing rich information on the cellular dynamics (Figure 4).[13]

2.3 Suppression of cellular autofluorescence and photodamage by NIR light sources

The advantages of UCNPs as imaging probes derive not only from the optical and chemical nature of the nanoparticles but also from the use of a NIR light source for exciting the UCNPs. First, NIR photons are not well absorbed by most biomolecules. In particular, the wavelength range of 750–900 nm is considered a spectrally transparent window with the smallest absorption cross section (*i.e.*, extinction coefficient, which is proportional to the absorbance) of the biomolecules in cells.[20] The wavelength of 980 nm does not fall within this range, and it shows a slightly larger absorption cross section because the onset of the vibrational transition of H_2O molecules is around 980 nm, and its intensity increases at longer wavelengths. However, the absorption cross section at 980 nm is only one order of magnitude larger than that in the transparent window (*i.e.*, 750–900 nm) and is still very much lower than those in the UV, visible, and IR spectral ranges. Thus, absorption by water molecules at 980 nm may not be sufficiently critical to cause problems in most cases. In fact, a few studies have investigated the effect of 980-nm excitation on cellular imaging.[13,21] The advantages of 980-nm excitation found in those studies are (1) the absence of autofluorescence and (2) a low level of cellular photodamage. Autofluorescence is the photoluminescence (fluorescence in general) resulting from excitation of natural cellular molecules that contributes to the background and competes with the signal from the probe we want to detect. Especially when

the signal intensity of the luminescent probe is not overwhelming, the background autofluorescence causes significant problems in analyzing the probe signals. Autofluorescence is usually generated in the visible spectral range, so we cannot intrinsically avoid its adverse contributions to images. However, with 980-nm or, more generally, NIR excitation, there is essentially no absorption by the biomolecules in the cell, as noted above; therefore, there should be no detectable autofluorescence.[5,13] As a result, overall the images display a very high level of contrast, so even a single UCNP can readily be observed with a very low background signal.[13]

Another advantage of using a NIR laser is that the photoinduced physical and chemical degradation of biomolecules is minimized. Photodamage generally originates from irreversible chemical reactions occurring in the excited states upon photon absorption. As mentioned above, in the NIR spectral region, absorption by biomolecules and H_2O is minimized, which indicates that the NIR excitation scheme in UCNP imaging effectively bypasses the first step in photodamage, namely, dumping excess energy to biological systems through photon absorption.[20] This noninvasive characteristic of NIR lasers has been discussed intensively in the field of biological imaging, and a few research groups recently confirmed that UCNPs do not induce noticeable photodamage even under harsh conditions.[13,21]

2.4 Versatile platform for wide-field two-photon microscopy

We have reviewed the benefits of using the novel imaging probe, UCNPs, especially from the perspective of cellular imaging. They are bright (detectable at the single-particle level), optically stable (nonblinking and nonbleaching), and biologically compatible (low cytotoxicity). The NIR laser used for excitation of these probes is noninvasive to cells and induces very little cellular autofluorescence. All these advantages can be integrated into and embodied in single UCNP particles, each of which can be used as a probe for wide-field two-

photon imaging. They can be used as labels for biomolecules such as nucleic acids and proteins in cells or as drug carriers. In both cases, what is important is that this UCNP-based imaging platform exhibits all the merits of conventional two-photon microscopy while simultaneously overcoming its drawbacks. In other words, it can be used for long-term continuous tracking of cellular dynamics, either slow or fast, using wide-field imaging techniques such as TIRF and epi-fluorescence microscopy. With this platform at hand, all we have to do is to endow UCNPs with the appropriate functions required for specific purposes using surface functionalization, namely, conjugation of functional biomolecules. These are necessary for the UCNPs to bind target molecules with high specificity and selectivity. Interestingly, the transitions responsible for the multiple emission bands are spectrally well separated, and each transition might be designed to perform different roles simultaneously. For example, one can use the green bands of $NaYF_4/Yb^{3+},Er^{3+}$ to monitor the location of the UCNP-biomolecule complex and the red band to monitor the binding or dissociation of biomolecules and UCNPs using FRET. Those studies will extend the scope of information on the mechanism of biochemical reactions.

We should note at this point that there is still room for improvement in this promising imaging platform. First, UCNPs need to be smaller because the typical UCNPs used in most studies to date are tens of nanometers in diameter, which is quite bulky, especially when they are used to label biomolecules a few nanometers in size. As for synthesis, miniaturizing particle sizes to smaller than or comparable to those of biomolecules is nothing but controlling the reaction conditions. However, such efforts will face difficulties because they are intrinsically accompanied by a decrease in the upconversion efficiency. This is due mostly to the reduction in the number of dopant cations in the UCNPs, which scales inversely with volume, and partly to the decreased crystal field on Yb^{3+} and Er^{3+} in smaller nanoparticles. Fortunately, Cohen *et al*. recently reported methods of synthesizing small

UCNPs of <10 nm in diameter that were still bright enough to be detected at the single-particle level.[6] This is a very promising result, and efforts to further reduce the particle size will make this system a more attractive and powerful platform for advanced bioimaging. To preserve or enhance the upconversion photoluminescence of smaller UCNPs may require a more profound understanding of the photophysics by which one can increase the absorption cross section and quantum yield. The second barrier is the biochemical surface functionalization. The coating material and conjugation of the biological moiety that allows more specific and selective interaction with the target cellular molecules are obviously of utmost importance in this field. Although a number of schemes for surface functionalization have been reported, their practical applications are strongly system-dependent. The development of a surface functionalization technology that is simultaneously universal and specific is crucial for finalizing the establishment of a versatile UCNP-based platform for wide-field two-photon imaging.

3. Multimodal *in vivo* imaging

3.1 Luminescence imaging

As described in the previous sections, the unique optical properties of UCNPs, such as the lack of background autofluorescence and low photodamage, are advantageous for *in vivo* luminescence imaging. The NIR excitation source offers an increased signal-to-background ratio, resulting in high imaging contrast. Cheng *et al.* compared the *in vivo* imaging sensitivity of UCNPs and QDs.[22] Mice were subcutaneously injected with UCNPs ($NaYF_4$:Er^{3+},Yb^{3+}) and QDs (QD 545 and QD 625) at various nanoparticle concentrations and then imaged. The results showed that the *in vivo* detection sensitivity of the UCNPs is one order of magnitude higher than that of the QDs. In addition, NIR light also increases the tissue penetration depth because of the low absorption of NIR by the biological environment,

which is very important for noninvasive animal imaging. When 800-nm emitting Tm^{3+}-doped UCNPs were tested, the imaging depth in a tissue phantom was ~600 μm in two-photon laser scanning microscopy and ~400 μm in two-photon wide-field microscopy, which is at least twice the depth for visible-light emitting fluorophores.[23]

Over the last decade, there have been numerous reports on *in vivo* luminescence imaging using UCNPs. Several papers on the biodistribution of UCNPs reported different distribution patterns of UCNPs in the body depending on the size and surface coating.[24] For example, poly(acrylic acid)-coated UCNPs were imaged *in vivo* for more than 7 days to monitor the long-term *in vivo* distribution of the nanoparticles; the results showed that the injected UCNPs were excreted through the liver and spleen. The *in vivo* distribution of nanoparticles during luminescence imaging was also confirmed using elemental analysis measurement (inductively coupled plasma atomic emission spectroscopy), demonstrating the usefulness of UCNPs for noninvasive whole-body imaging. Targeted tumor imaging was also successfully demonstrated by conjugation of targeting peptides or antibodies.[24] Cyclic-RGD-peptide-conjugated UCNPs showed a high signal-to-noise ratio (~24) between the tumor and its background. The high sensitivity of UCNPs can also be applied to *in vivo* stem cell tracking.[25] UCNP-labeled mesenchymal stem cells were subcutaneously transplanted into mice, and images were acquired using the Maestro *in vivo* imaging system. About 10 UCNP-labeled cells could be detected; this detection limit is lower by at least 2 orders of magnitude than that of QDs or MRI contrast agents. Further, the emission intensity changes depending on the number of cells. The high sensitivity and photostability of UCNPs can play an important role in following the translocation of implanted stem cells. After UCNP-labeled mesenchymal stem cells were injected intravenously, their temporal translocation from the lung to the liver could be monitored for 24 h.

Multiplexing is a unique characteristic of the luminescence imaging modality and makes it possible to measure different targets accurately and simultaneously. The emission wavelength of QDs can be tuned by controlling the particle size. Although fine-tuning the particle size of QDs is difficult, UCNPs are preferable to QDs for multiplexing because the emission wavelength of UCNPs can be easily tuned by varying the dopant ions rather than the particle size, as in QDs. The characteristic emission of UCNPs is determined by the ladder-like atomic energy level of each lanthanide dopant ion; therefore, the preparation of UCNPs with different sharp emission peaks is feasible simply by doping with the corresponding lanthanide ion. There are several reports on the tuning of upconversion luminescence. First, by changing the emitter dopant, the emission wavelength can be changed from the UV to the NIR. When Er^{3+} or Ho^{3+} is co-doped as an emitter, the UCNPs emit green and red light, whereas Tm^{3+}-doped UCNPs emit blue and NIR (800-nm) light. In addition, the emitted color can be tuned by combining different types of emitter ions, in which the resulting color is determined through the relative ratio of green, red, and blue emission. Second, the emission wavelength can be tuned using energy transfer between UCNPs and dyes (Figure 5a).[26] If the absorption band of the dyes matches the emission band of the UCNPs, the dye on the surface of the UCNPs can be activated by 980-nm irradiation through energy transfer from the UCNPs to the dyes. By incorporating different types of dyes into UCNPs, multicolor-emitting UCNPs could be synthesized. *In vivo* multicolor imaging using a UCNP-dye combination was also successfully demonstrated after spectral unmixing using the modified Maestro *in vivo* imaging setup (Figure 5a).[26] The Liu group recently suggested using energy migration among the emitter ions for upconversion luminescence tuning (Figure 5b).[27] The UCNPs have a core–shell structure, in which the core is UCNPs ($NaGdF_4$:Tm^{3+},Yb^{3+}) and the shell is $NaGdF_4$:X^{3+} (X^{3+}: emitter ions such as Dy^{3+}, Tb^{3+}, Eu^{3+}, and Sm^{3+}). The energy excited in Tm^{3+} from Yb^{3+} ions in the core is transferred to emitter ions (X^{3+}) in the shell through Gd^{3+}

sublattice-mediated energy migration. The separation of Tm^{3+} and other emitter ions (X^{3+}) also reduces unnecessary cross-relaxation, resulting in efficient upconversion luminescence. As shown in Figure 5b, UCNPs with various emission wavelengths could be synthesized by changing the emitter in the shell. Compared to the UCNP-dye combination mentioned above, energy migration between the emitters in $NaGdF_4:Tm^{3+},Yb^{3+}@NaGdF_4:X^{3+}$ produced a very sharp emission peak, minimizing the spectral overlap. However, their complicated energy transfer mechanism, including excitation by more than five NIR photons, can induce the low luminescence efficiency. Instead of color tuning, multiplexing through tuning the lifetime of UCNPs was reported very recently (Figure 5c).[28] Different distances between the sensitizers and emitters changes the lifetime of UCNPs. In 40-nm Tm^{3+}-doped UCNPs, the lifetime can be tuned from 48 μs (4 mol% Tm^{3+}) to 668 μs (0.2 mol% Tm^{3+}). Because a shorter distance between Yb^{3+} and Tm^{3+} induces cross-relaxation, the high Tm^{3+} content shortens the luminescence lifetime. Pseudocolor images using a time-resolved detection method suggest a new type of optical multiplexing. However, the time-resolved imaging setup will be necessary for tunable lifetime multiplexing. And, in the multiplexing using UCNPs, the different luminescence intensities of the UCNPs with different emission wavelength and lifetime may induce the error for decoding mixed spectra and lifetimes. For more accurate decoding, it may be considered to control the concentration of the different types of UCNPs in order to give comparable emission intensities among them.[28]

Despite their successful demonstration in animal imaging, the development of a new type of UCNPs for *in vivo* imaging is needed. Conventional Yb^{3+}-doped UCNPs are excited by a 980-nm laser because Yb^{3+} has strong absorption near 980 nm. As discussed in the previous section, absorption by water molecules at 980 nm may not cause any significant photodamage in most cellular imaging cases. However, heating by a 980-nm laser can cause thermally induced cell death and tissue damage because the 980-nm laser is usually used at high power

for *in vivo* imaging. For this reason, a 915-nm laser has been used instead of a 980-nm excitation source, with a sacrifice in emission efficiency.[29] Nd^{3+} was recently introduced to UCNPs as a new sensitizer because it has a sharp absorption band around 800 nm.[30] Because the energy transfer from Nd^{3+} to Yb^{3+} is highly efficient, Nd^{3+} can be used to excite emitters (Er^{3+}, Tm^{3+}, and Ho^{3+}) through Yb^{3+}. The excitation wavelengths of Nd^{3+} are shorter than that of Yb^{3+} (980 nm), and the absorption by water molecules around 800 nm is much lower than that at 980 nm (Figure 6a). The Yan group reported the synthesis of Nd^{3+}-doped UCNPs ($NaGdF_4$:Er^{3+},Yb^{3+}@$NaGdF_4$:Yb^{3+},Nd^{3+}), which can be activated by an 808-nm laser (Figure 6b).[30] Nd^{3+} ions in the shell of the UCNPs absorb an 808-nm photon to the $^4F_{5/2}$ state and then relax to the $^4F_{3/2}$ state by a nonradiative pathway. The excited energy could be transferred to the $^2F_{5/2}$ state of a neighboring Yb^{3+}, and then upconversion between Yb^{3+} and Er^{3+} occurs. Because Nd^{3+} ions feature a larger absorption cross section (1.2×10^{-19} cm^2 at 808 nm) in the NIR region than Yb^{3+} (1.2×10^{-20} cm^2 at 980 nm), and energy transfer from Nd^{3+} to Yb^{3+} is highly efficient, the resulting UCNPs exhibit a high upconversion efficiency under 808-nm excitation.[30] This efficient emission from Nd^{3+}-doped UCNPs was also demonstrated in a mouse imaging experiment (Figure 6c). Subcutaneously injected Nd^{3+}-doped UCNPs showed nearly the same photon flux as common UCNPs. More importantly, the use of an 808-nm light source dramatically decreased the overheating effect (Figure 6d). At a power density of 130 mW/cm^2, the temperature rise under 980-nm irradiation for 50 s was ~7 °C, whereas that under 808-nm irradiation for 300 s was ~1 °C. The reduction in local overheating is beneficial for minimizing tissue damage during continuous *in vivo* imaging. Changing the emitter ions from Er^{3+} to Tm^{3+} can produce 800-nm emitting Nd^{3+}-doped UCNPs under 808-nm excitation, minimizing the laser toxicity and maximizing the *in vivo* imaging capability.

3.2 Magnetic resonance imaging

As described above, doping is critical to control the crystal structures and optical properties of UCNPs. Among lanthanide dopant ions, Gd^{3+} ions have been used to increase the emission efficiency by inducing crystal phase transformations.[11] Doped Gd^{3+} ions in UCNPs can also serve as the T_1 MRI contrast-enhancing element. Because of the seven unpaired 4f electrons, Gd complexes such as Gd-DTPA are typical MRI contrast agents for imaging blood vessels, and Gd^{3+}-based nanoparticles were recently investigated as potential T_1 MRI contrast agents.[31] Consequently, Gd^{3+}-doped UCNPs are considered as inherently promising dual-modal imaging probes for combining luminescence imaging and MRI.

To introduce MRI modality into UCNPs, several research groups have suggested a strategy of Gd^{3+} co-doping into a UCNP host matrix. Kumar *et al.* reported that Gd^{3+} co-doped UCNPs ($NaYF_4$:2%Er^{3+},10%Yb^{3+},10%Gd^{3+}) have potential for optical and MR imaging (relaxivity r_1 = 0.14 $mM^{-1}s^{-1}$).[32] The Li group also demonstrated the T_1 MRI capability of Gd^{3+} co-doped UCNPs ($NaYF_4$:2%Er^{3+},18%Yb^{3+},60%Gd^{3+}) by imaging the liver and spleen in mice (r_1 = 0.405 $mM^{-1}s^{-1}$).[33] However, the low relaxivities of Gd^{3+} co-doped UCNPs hamper their wide application in diagnostics. Gd^{3+} ions are distributed in the entire particle volume, and the ratio of active Gd^{3+} ions exposed on the surface is very low. The relaxivity (r_1) could be increased from 0.14 $mM^{-1}s^{-1}$ to 0.405 $mM^{-1}s^{-1}$ by changing the Gd^{3+} doping amount from 10% to 60%, showing that the low relaxivity of Gd^{3+} co-doped UCNPs is due to the low Gd^{3+} dopant concentration. A very high r_1 value (r_1 = 28.39 $mM^{-1}s^{-1}$) was recently achieved by doping Gd^{3+} ions only on the particle surface, where they were synthesized using cation exchange between Gd^{3+} ions and Y^{3+} ions on the surface of UCNPs.[34]

Instead of Gd^{3+} co-doping, a Gd^{3+}-based host matrix ($NaGdF_4$) was also used for the MRI modality.[5] $NaGdF_4$ UCNPs ($NaGdF_4$:2%Er^{3+},20%Yb^{3+}@$NaGdF_4$) exhibited a higher r_1 value (r_1 = 1.40 $mM^{-1}s^{-1}$) than Gd^{3+} co-doped UCNPs. Compared to the Gd^{3+} co-doped system, the

$NaGdF_4$ host matrix has many more Gd^{3+} ions exposed to water molecules. However, their T_1 contrast enhancement is not sufficient for clinical use because the r_1 value is still lower than that of Gd-DTPA (5–6 $mM^{-1}s^{-1}$). To achieve a higher r_1 value, a Gd^{3+}-free UCNP core with a $NaGdF_4$ shell structure was suggested.[35] Because Gd^{3+} ions near the particle surface are mainly responsible for shortening the T_1 relaxation time of water molecules, control of the $NaGdF_4$ shell thickness made it possible to increase the r_1 value to 6.18 $mM^{-1}s^{-1}$.[36] The detailed relaxivity mechanism recently reported by the Shi group[37] revealed that the relaxation shortening depends on the surface modification method, such as silica coating, as well as the $NaGdF_4$ shell thickness (Figure 7a). For instance, the outer-sphere r_1 relaxivity mechanism can be applied to understand silica-coated UCNPs. The higher mobility of the outer-sphere water molecules decreases the correlation diffusion time, resulting in a reduced outer-sphere r_1 relaxivity. A mesoporous silica shell with more permeable pores did not cause any significant change in the r_1 value, whereas the use of a dense silica shell with less water-permeable micropores changed both the r_1 and r_2 values because water molecule diffusion is restricted to the microporous channels in the dense silica. Ligand-free UCNPs, in which oleic acid capping molecules were removed by protonation in acidic solution, can be explained by both inner- and outer-sphere mechanisms. In ligand-free UCNPs, water molecules can bond directly with surface Gd^{3+} ions, resulting in the highest r_1 value (14.73 $mM^{-1}s^{-1}$) among $NaGdF_4$-shell-coated UCNPs. On the basis of the understanding of the relaxivity mechanism, the properties of UCNPs can be tuned for T_1 or T_2 MRI by optimizing the $NaGdF_4$ shell thickness and surface modification. $NaGdF_4$-based UCNPs could be used to enhance the T_1 contrast of tumors in the mouse model by the enhanced permeability and retention effect (Figure 7b).[35]

Superparamagnetic UCNPs have also been developed as T_2 MRI contrast agents. To introduce superparamagnetism, magnetic iron oxide nanoparticles were usually assembled on

the UCNPs, or the two components were encapsulated in polymer micelles. Cheng *et al.* reported the preparation of multifunctional nanoprobes consisting of iron oxide nanoparticles assembled on UCNPs.[38] However, the overall size of the resulting probes is too large for use by systemic administration. The Li group synthesized UCNP core–iron oxide shell nanoparticles by growing a 5-nm Fe_xO_y shell on an as-synthesized $NaYF_4:Tm^{3+},Yb^{3+}$ core (Figure 7c).[39] The saturation magnetization (M_s) of the resulting core–shell nanoparticles is about 12 emu/g, and the r_2 value is 189 $mM^{-1}s^{-1}$, which is higher than that of a conventional T_2 MRI contrast agent (r_2 = 108 $mM^{-1}s^{-1}$). The T_2 MRI images demonstrate successful imaging of the lymph node (Figure 7d). Zhong *et al.* synthesized superparamagnetic UCNPs by forming a $NaYF_4:Er^{3+},Yb^{3+}$ shell on the seed Fe_3O_4 nanoparticles.[40] The M_s (1.1 emu/g) of the resulting core–shell UCNPs was lower than that of the seed Fe_3O_4 nanoparticles (20.5 emu/g), which may be the result of the thick $NaYF_4$ shell (~11 nm). The superparamagnetic UCNPs prepared by the two methods exhibited significantly reduced emission intensity because the excitation and emission light are absorbed by the iron oxide nanoparticles.

3.3 Computed tomography

CT is one of the most common imaging modalities in clinical use to diagnose disease and monitor treatment because of its reasonable cost and deep tissue penetration capability. Lanthanide elements can be used as CT contrast agents owing to their high X-ray attenuation. Therefore, instead of the widely used $NaYF_4$, various lanthanide host materials with high atomic numbers have been designed for CT contrast enhancement. For instance, Yb^{3+}-based UCNPs ($NaYbF_4:Er^{3+}$) showed a higher contrast effect than a clinically used iodinated contrast agent.[41] Gd^{3+}-based UCNPs ($NaGdF_4:Er^{3+},Yb^{3+}$), which were mentioned in the MRI section, can also be used for CT, suggesting that $NaGdF_4:Er^{3+},Yb^{3+}$ UCNPs can be a trimodal imaging probe for optical imaging, MRI, and CT.[42] $NaLuF_4$ UCNPs were recently developed

for more efficient CT imaging because Lu^{3+} ions have the highest atomic number among lanthanide elements. These UCNPs exhibited almost five-fold higher contrast effects than the commercial iodinated agent, and their long circulation time and low toxicity compared to commercial agents make them a highly promising CT agent.[43] *In vivo* CT imaging using $NaLuF_4$-based UCNPs could visualize tumors (Figure 8a–f).[43] Xiao *et al*. recently synthesized UCNPs decorated with tantalum oxide nanoparticles, which have been intensively investigated as a CT imaging contrast agent owing to their high X-ray attenuation and biocompatibility.[44] In addition, transparent tantalum oxide nanoparticles do not quench the upconversion luminescence, unlike gold nanomaterials, which have also been studied as CT contrast agents.

3.4 Positron emission tomography and single-photon emission computed tomography

PET can have a synergistic effect when combined with other imaging modalities such as MRI and CT because PET has extremely high sensitivity at the picomolar level. Common multimodal imaging nanoprobes combined with PET have generally been prepared by attaching radioactive isotopes to nanoparticles. The radioactive ions may be released from the particle, which can lead to misinterpretation of the results. Liu *et al*. recently demonstrated that ^{18}F-labeled UCNPs can be prepared by cation-assisted ligand assembly.[34] Radioactive $^{18}F^-$ ions could be incorporated into a $NaYF_4$ matrix via reactions with Y^{3+} or Gd^{3+}, and the liver and spleen could be visualized in 10 min after the ^{18}F-labeled UCNPs were injected (Figure 8g).

Single-photon emission computed tomography (SPECT) can also be added as an additional modality in lanthanide-based UCNPs. As described in the previous sections, doping lanthanide ions into the $NaYF_4$ matrix is very easy. By adding $^{153}Sm^{3+}$ ions to UCNPs, the SPECT modality can be simply added.[45] Sun *et al.* synthesized a multimodal probe that has a

$NaLuF_4$:Yb^{3+},Tm^{3+} core and $NaGd_{1-x}(^{153}Sm)_xF_4$ shell and could be used for SPECT/CT imaging (Figure 8h). They demonstrated that the probe could work as a quadruple-modal imaging agent for NIR-to-NIR imaging (Yb^{3+}, Tm^{3+}), CT (Lu^{3+}, Yb^{3+}), T_1 MRI (Gd^{3+}), and SPECT ($^{153}Sm^{3+}$).

4. Multifunctionality for imaging and therapy

UCNPs that are stimulated by NIR light are considered a potential tumor therapy. NIR light can induce local treatment, whereas the prognosis of the lesion can be estimated using other imaging modalities such as MRI or CT. Visible light emission from UCNPs by NIR excitation have been applied to photodynamic therapy (PDT). A typical PDT drug is activated by visible light and then produces reactive oxygen species, which kill the target cells. When UCNPs are used for PDT, NIR light can activate the PDT drug, which leads to greater penetration depth and higher therapeutic efficacy. Park *et al.* showed that Ce6-conjugated UCNPs could treat a tumor lesion through systemic administration.[35] Later, the Zhang group synthesized mesoporous-silica-coated UCNPs loaded with dual photosensitizers (Figure 9a).[46] The two types of photosensitizers are activated by green and red emission from UCNPs ($NaLuF_4$:Yb^{3+},Er^{3+}), and the UCNPs showed a much higher PDT efficiency than a single-photosensitizer system, which was also demonstrated in a mouse tumor model (Figure 9b).

For photothermal therapy (PTT), NIR light can be used directly to induce target cell death by increasing the temperature. Gold nanoshells and gold nanorods have been widely used for PTT because they have a large absorption cross section in the NIR region and they efficiently convert the absorbed radiation into heat, which causes target cell destruction. Cheng *et al.* synthesized a UCNP@Fe_3O_4@gold structure for multifunctionality, and the nanocomposite showed an advantage for magnetic targeted PTT. CuS-nanoparticle-decorated UCNPs

recently showed potential for PTT owing to their low cost and high photothermal conversion efficiency (Figure 9c and d).[47] The Shi group reported that PTT and radiation therapy were combined for synergistic therapy because UCNPs enhance the radiation dose owing to the heavy lanthanide elements. The synergistic therapeutic effect was also demonstrated in an *in vivo* model.

NIR light can also control anticancer drug activities and their release for efficient therapy. The Lin group recently reported platinum-prodrug-conjugated UCNPs for NIR-triggered drug activation and release.[48] For prodrug activation, UV-emitting UCNPs ($NaYF_4:Yb^{3+},Tm^{3+}@NaGdF_4:Yb^{3+}$) were synthesized, and a platinum(IV) prodrug, *trans,trans,trans*-$[Pt(N_3)_2(NH_3)(py)(O_2CCH_2CH_2COOH)_2]$, was conjugated on the UCNPs (Figure 9e). Optical imaging (NIR to NIR), MRI, and CT were used to determine the tumor location, and tumor growth was successfully inhibited in the mouse tumor model (Figure 9f).

5. Conclusion

In this tutorial, the versatility of UCNPs as a platform for both wide-field two-photon microscopy and multimodal *in vivo* imaging was described. Owing to their unique optical properties, which include resistance to photoblinking and photobleaching, minimal background autofluorescence, and low photoinduced toxicity, upconverting nanomaterials have been attracting attention as promising bioimaging probes for both *in vitro* and *in vivo* use. In addition, recent advances in synthetic methods for UCNPs have improved their luminescence efficiency while decreasing their overall size to less than 10 nm. Therefore, UCNPs fulfill the prerequisites for biological application, and they are actively used in the field of imaging and therapy. The UCNP-based platform for wide-field two-photon microscopy enables continuous real-time imaging of subcellular events at a higher frame rate than that of conventional two-photon confocal microscopy. UCNPs could also be monitored

in live cells for long-term tracking of a specific target. Their advantages are not limited to *in vitro* imaging. Fine tuning of the material composition allows *in vivo* multimodal imaging using UCNPs. Because the lanthanide elements have similar atomic sizes and chemical properties, a UCNP library with different compositions can easily be synthesized, enabling a combination of several imaging modalities. With current efforts to improve the properties of UCNPs, detailed basic studies on the biodistribution and long-term toxicity will be required for UCNPs to be widely used in the fields of biology and medicine.

Acknowledgements

T.H. acknowledges the financial support by the Research Center Program of the Institute for Basic Science (IBS) in Korea. Y.D.S. was supported by KRICT (SI-1408, KK-0904-02, OASIS Project), the Nano R&D Program (No. 2009-0082861) and the Public Welfare & Safety Research Program (2011-0020957) through the NRF of Korea funded by the Ministry of Science, ICT, and Future Planning (MSIP, Korea), and the Industrial Strategic Technology Development Program (nos. 10033183 and 10037397) funded by the Ministry of Trade, Industry, and Energy (MI, Korea). K.T.L. was supported by the Basic Science Research Program of NRF (NRF-2013R1A1A1058451) and the Global University Projects of GIST (K03954). We are also grateful to Dr. Jeong Hyun Kim, Dr. Hyung Min Kim, Dr. Sang Hwan Nam, Dr. Yun Mi Bae, Byeongjun Yoo, and Dr. Ki-Seok Jeon for their productive collaboration and discussion.

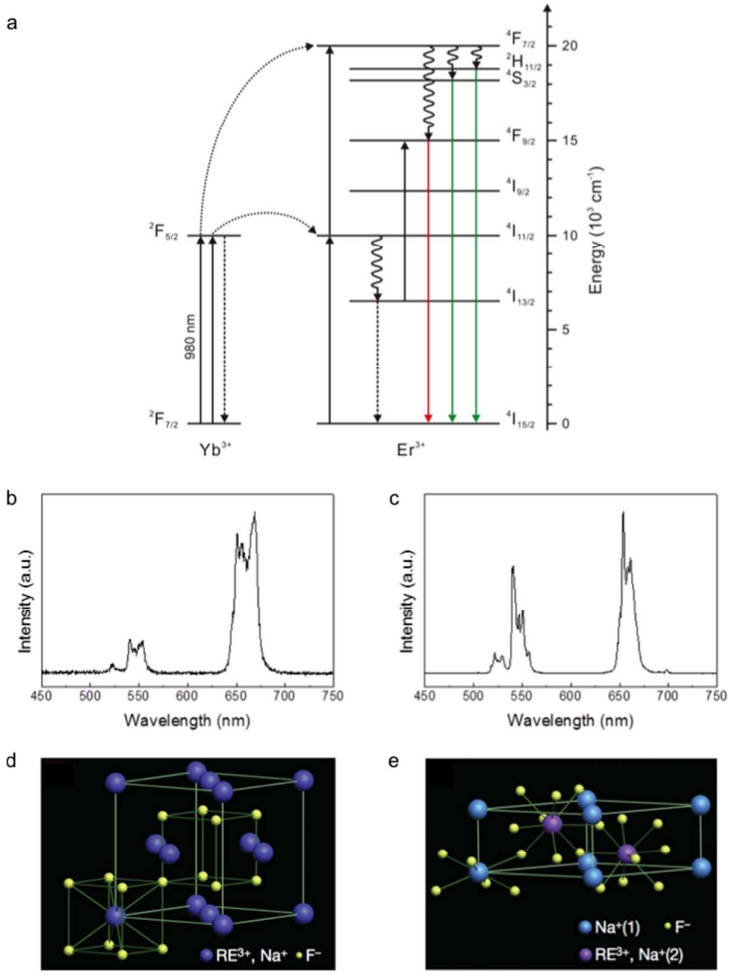

Figure 1. (a) Schematic diagram of upconversion processes in $NaYF_4$:Yb^{3+},Er^{3+}. The solid arrows indicate excitation and emission. The dotted, dashed, and wavy arrows represent energy transfer, nonradiative transition, and multiphonon relaxation, respectively. (b-c) Photoluminescence spectra of $NaYF_4$:Yb^{3+},Er^{3+} UCNPs with different crystal structures in hexane under 980-nm excitation. (b) Cubic and (c) hexagonal phase $NaYF_4$:Yb^{3+},Er^{3+} UCNPs. (d-e) Schematic illustration of cubic (d) and hexagonal (e) phase $NaREF_4$ crystal structures. Adapted with permission from ref. 8. (Copyright 2013 American Chemical Society), and ref. 11 (Copyright 2010 Macmillan Publishers Ltd), respectively.

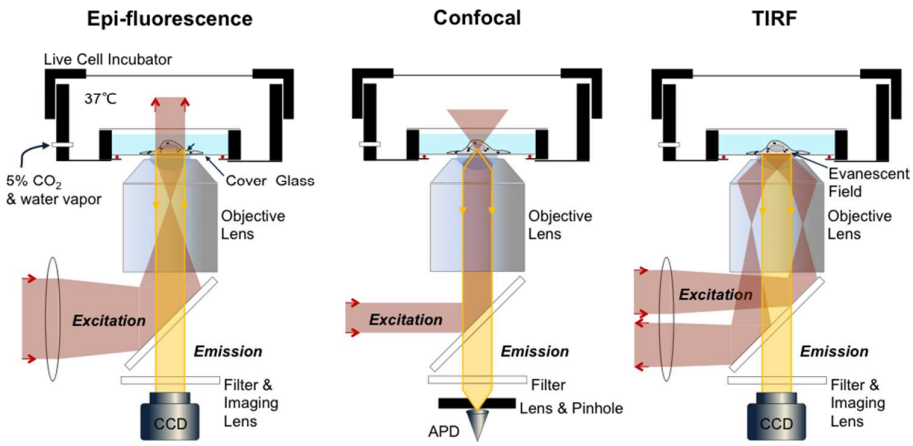

Figure 2. Fluorescence-based microscopy techniques. (a) Epi-fluorescence microscopy. (b) Confocal microscopy. (c) TIRF (total internal reflection fluorescence) microscopy.

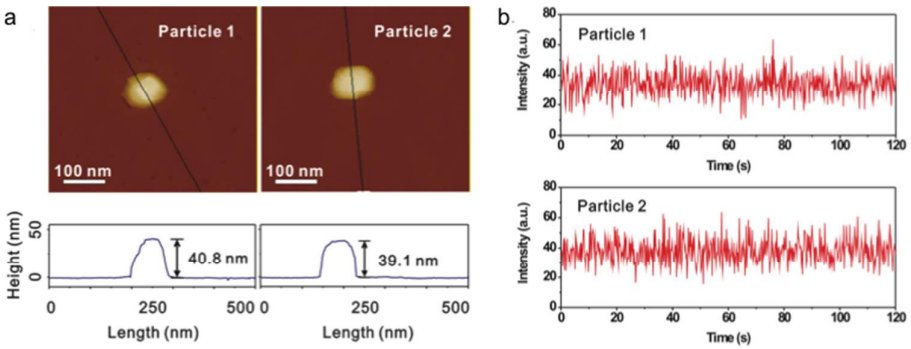

Figure 3. Single-particle measurements of UCNPs. (a) (top row) AFM images of the single UCNPs (cubic phase $NaGdF_4:Er^{3+},Yb^{3+}@NaGdF_4$) and (bottom row) the result of section analysis. (b) The luminescence time traces of the particles **1** and **2** acquired with 200 ms time bins. Adapted with permission from ref. 5. Copyright 2009 WILEY-VCH Verlag GmbH & Co. KGaA.

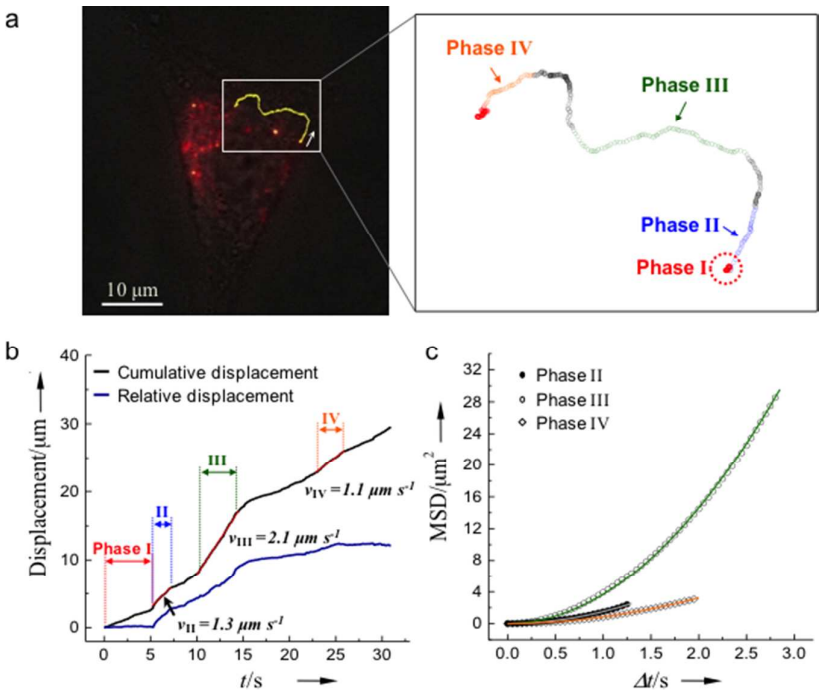

Figure 4. (a) A trajectory of a UCNP (hexagonal phase $NaYF_4$:Er^{3+},Yb^3) transported by motor proteins such as dyneins. (b) Cumulative and relative displacement traces for the trajectory shown in (a). (c) MSDs (mean square displacement = $\langle \boldsymbol{r}^2 \rangle$ where $\boldsymbol{r}$ is the distance that the particle moves during a time interval, Δt) for phases II–IV. These are fit to the quadratic functions of Δt ($4D\Delta t + v^2\Delta t^2$), which is indicative of the two-dimensional active transport of a vesicle-encapsulated UCNP by motor proteins. Adapted with permission from ref. 13. Copyright 2011 WILEY-VCH Verlag GmbH & Co. KGaA.

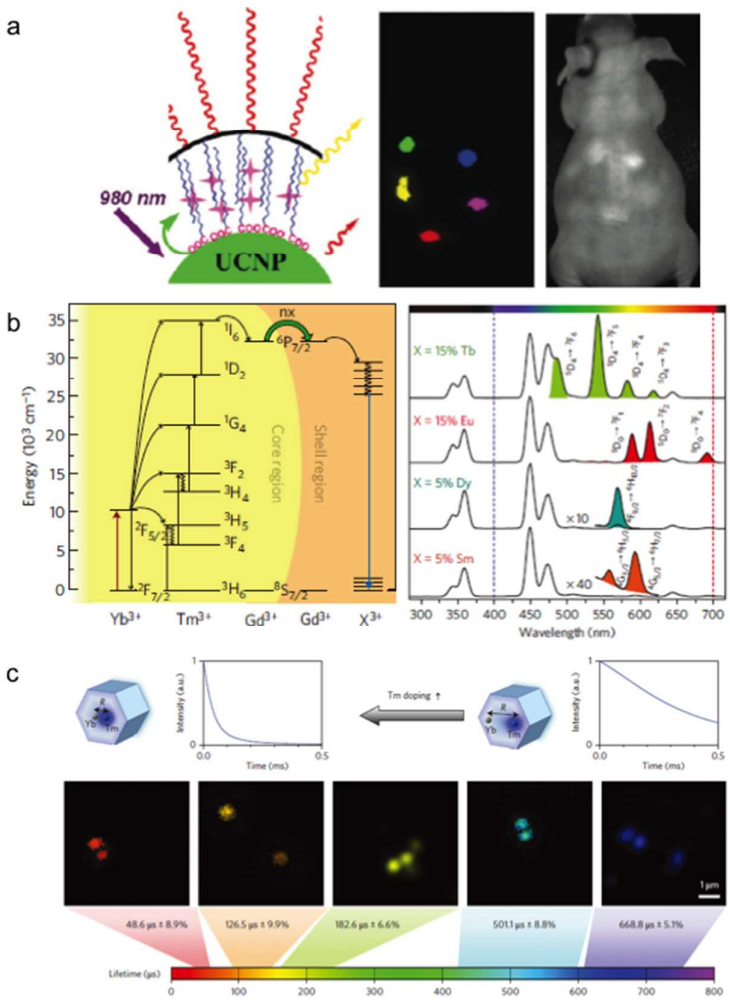

Figure 5. (a) (left) Schematic of multicolor emission from UCNP-dye system. (middle) *In vivo* multicolor image of nude mouse subcutaneously injected with five different kinds of UCNP-dye solutions after spectral unmixing. (right) Bright field image of the mouse. (b) Tuning of upconversion luminescence through energy transfer in core@shell structure. Left is energy diagram, and right is the emission spectra of the UCNPs with different activator (X^{3+}) in shell. (c) Tuning of upconversion lifetime and time-resolved images of UCNPs ($NaYF_4$:Tm^{3+},Yb^{3+}). The different colors indicate different lifetime values decoded from a decay curve. As the ratio of Tm^{3+}-to-Yb^{3+} decreases, their lifetime increases. Adapted with permission from ref. 26 (Copyright 2011 American Chemical Society), ref. 27 (Copyright 2011 Macmillan Publishers Ltd), and ref. 28 (Copyright 2014 Macmillan Publishers Ltd), respectively.

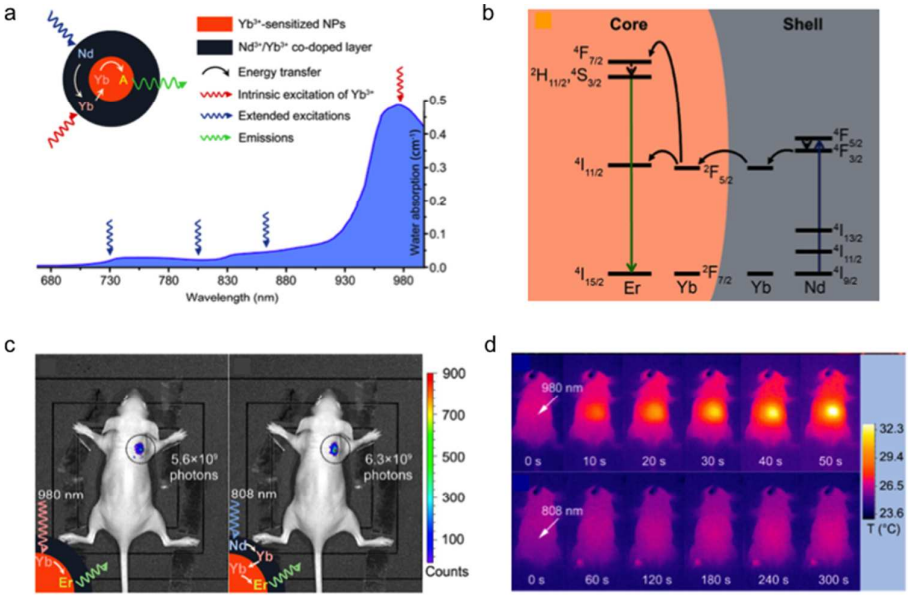

Figure 6. (a) Schematic illustration of Nd^{3+}-doped UCNPs and absorption spectrum of water in the NIR region. (b) Diagram of energy transfer in the core/shell structured UCNPs under 808-nm excitation. (c) Luminescence images of mice subcutaneously injected with common UCNPs (left) and Nd^{3+}-doped UCNPs (right), under 980-nm (left) and 808-nm (right) irradiation, respectively. (d) Thermal images of mice under 980-nm laser for 50 s (top row) and 808-nm laser for 300 s (bottom row). Adapted with permission from ref. 30. Copyright 2013 American Chemical Society.

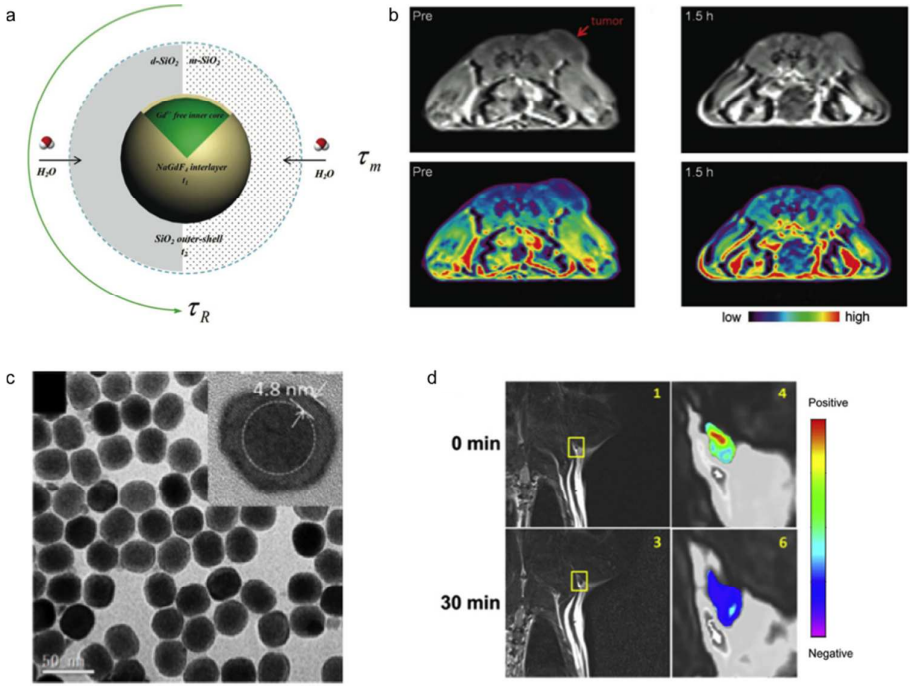

Figure 7. (a) MRI relaxivity mechanism of UCNP@$NaGdF_4$@silica. UCNP core is Gd^{3+}-free, and $NaGdF_4$ layer is responsible for MRI contrast enhancement. Dense (d-SiO_2) and mesoporous (m-SiO_2) shell with different shell thickness were coated on the UCNPs to investigate the effect of coordinated water molecules, water residence time (τ_m), and rotational correlation time (τ_R). (b) *In vivo* MR images of tumor-bearing mice after intravenous injection of UCNPs ($NaYF_4$:Er^{3+},Yb^{3+}@$NaGdF_4$) with chlorin e6. The upper row is T1 images of before (left) and after (right) injection. The lower row is color-mapped images of upper row. (c) TEM image of $NaYF_4$:Tm^{3+},Yb^{3+}@Fe_xO_y. (d) MR images of the lymph node of rat after injection of $NaYF_4$:Tm^{3+},Yb^{3+}@Fe_xO_y. The left column is T2 MR images, and the right column is color-mapped images of yellow boxes in T2 MR images. Adapted with permission from ref. 37 (Copyright 2013 WILEY-VCH Verlag GmbH & Co. KGaA), ref. 35 (Copyright 2011 WILEY-VCH Verlag GmbH & Co. KGaA), and ref. 39 (Copyright 2011 Elsevier Ltd), respectively.

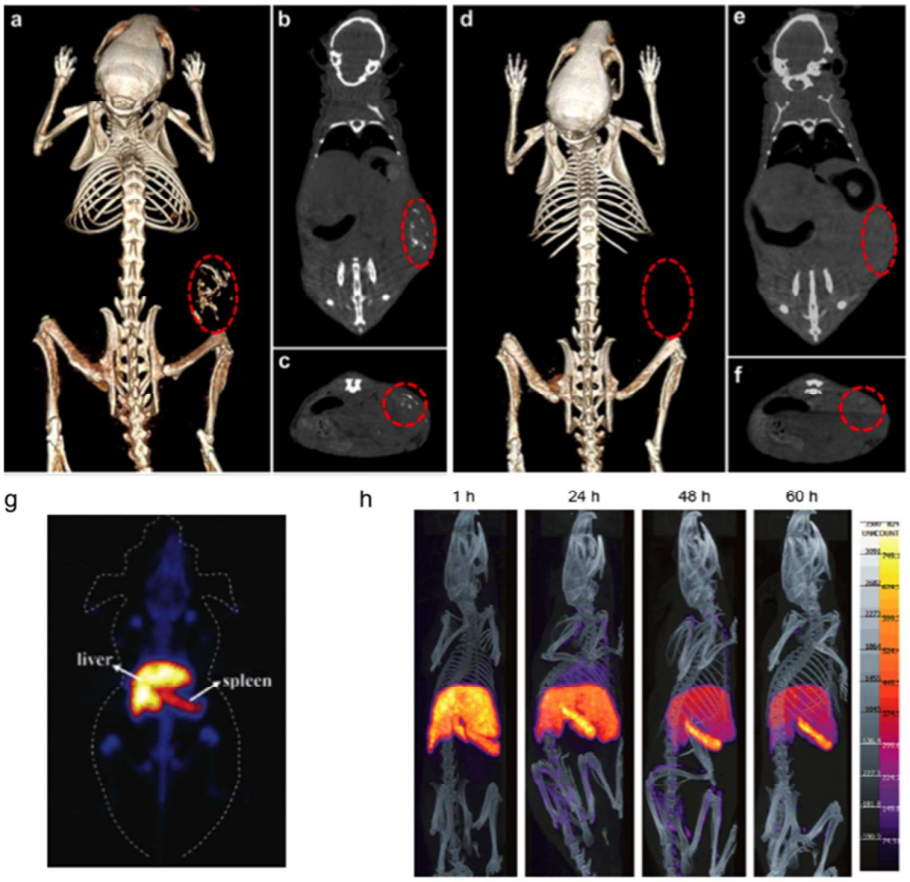

Figure 8. (a-f) CT images of tumor-bearing mice before (d-f) and 30 min after (a-c) intratumoral injection of Fe_3O_4@$NaLuF_4$:Yb^{3+},Er^{3+}/Tm^{3+} UCNPs. (a,d) CT volume-rendered images, (b,e) coronal and (c,f) transversal images of the mice. Red circles indicate the tumor positions. (g) PET image of mouse 10 min post-injection of ^{18}F-labeled UCNPs. (h) SPECT/CT images of mouse injected with $NaLuF_4$:Yb^{3+},Tm^{3+}@$NaGd_{1-x}(^{153}Sm)_xF_4$ UCNPs. Adapted with permission from ref. 43 (Copyright 2012 Elsevier Ltd), ref. 34 (Copyright 2011 American Chemical Society), and ref 45 (Copyright 2013 American Chemical Society), respectively.

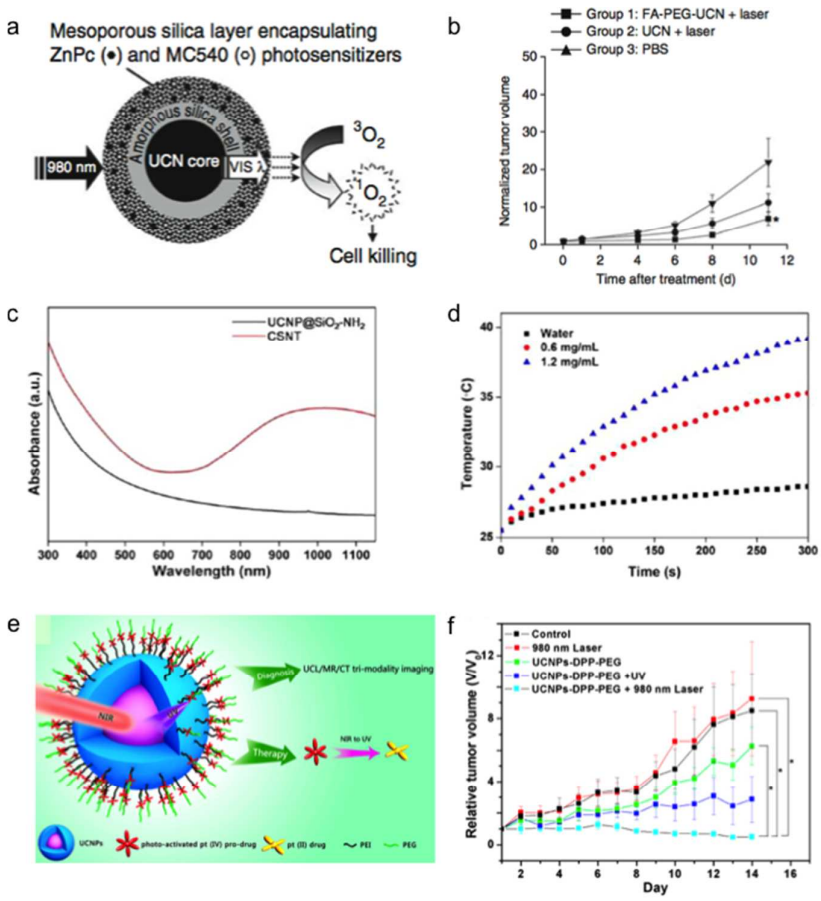

Figure 9. (a) Schematic illustration of photosensitizer-loaded UCNPs. UCNPs convert 980-nm light to visible light, which activates photosensitizers. (b) Change of tumor volume in tumor-bearing mice after intravenous injection of UCNPs. (c) Absorption spectrum of UCNP@SiO_2 and core-satellite nanotheranostic (CSNT, UCNP@CuS). (d) Temperature increase of UCNP@CuS solution under 980-nm laser (1.5 W/cm^2). (e) Schematic of UCNP-pro-drug. UCNPs convert NIR light to UV, which activates platinum(IV) pro-drug. (f) Change of tumor volume in tumor-bearing mice after intravenous injection of UCNP-pro-drug (DPP). Adapted with permission from ref. 46 (Copyright 2012 Macmillan Publishers Ltd), ref. 47 (Copyright 2013 American Chemical Society), and ref. 48 (Copyright 2013 American Chemical Society), respectively.

References

1. F. Auzel, *Chem. Rev.*, 2004, **104**, 139-173.
2. M. Haase and H. Schäfer, *Angew. Chem. Int. Ed.*, 2011, **50**, 5808-5829.
3. F. Wang, D. Banerjee, Y. Liu, X. Chen and X. Liu, *Analyst*, 2010, **135**, 1839-1854.
4. G. Chen and G. Han, *Theranostics*, 2013, **3**, 289-291.
5. Y. I. Park, J. H. Kim, K. T. Lee, K.-S. Jeon, H. B. Na, J. H. Yu, H. M. Kim, N. Lee, S. H. Choi, S.-I. Baik, H. Kim, S. P. Park, B.-J. Park, Y. W. Kim, S. H. Lee, S.-Y. Yoon, I. C. Song, W. K. Moon, Y. D. Suh and T. Hyeon, *Adv. Mater.*, 2009, **21**, 4467-4471.
6. A. D. Ostrowski, E. M. Chan, D. J. Gargas, E. M. Katz, G. Han, P. J. Schuck, D. J. Milliron and B. E. Cohen, *ACS Nano*, 2012, **6**, 2686-2692.
7. S. Gai, C. Li, P. Yang and J. Lin, *Chem. Rev.*, 2014, **114**, 2343-2389.
8. Y. I. Park, S. H. Nam, J. H. Kim, Y. M. Bae, B. Yoo, H. M. Kim, K.-S. Jeon, H. S. Park, J. S. Choi, K. T. Lee, Y. D. Suh and T. Hyeon, *J. Phys. Chem. C*, 2013, **117**, 2239-2244.
9. J. Zhao, Y. Sun, X. Kong, L. Tian, Y. Wang, L. Tu, J. Zhao and H. Zhang, *J. Phys. Chem. B*, 2008, **112**, 15666-15672.
10. J.-C. Boyer, L. A. Cuccia and J. A. Capobianco, *Nano Lett.*, 2007, **7**, 847-852.
11. F. Wang, Y. Han, C. S. Lim, Y. Lu, J. Wang, J. Xu, H. Chen, C. Zhang, M. Hong and X. Liu, *Nature*, 2010, **463**, 1061-1065.
12. F. Wang and X. Liu, *Chem. Soc. Rev.*, 2009, **38**, 976-989.
13. S. H. Nam, Y. M. Bae, Y. I. Park, J. H. Kim, H. M. Kim, J. S. Choi, K. T. Lee, T. Hyeon and Y. D. Suh, *Angew. Chem. Int. Ed.*, 2011, **50**, 6093-6097.
14. A. Jemal, R. Siegel, E. Ward, Y. Hao, J. Xu and M. J. Thun, *CA Cancer J. Clin.*, 2009, **59**, 225-249.
15. U. Resch-Genger, M. Grabolle, S. Cavaliere-Jaricot, R. Nitschke and T. Nann, *Nat. Methods*, 2008, **5**, 763-775.
16. Q. Zhan, S. He, J. Qian, H. Cheng and F. Cai, *Theranostics*, 2013, **3**, 306-316.
17. M. Nirmal, B. O. Dabbousi, M. G. Bawendi, J. J. Macklin, J. K. Trautman, T. D. Harris and L. E. Brus, *Nature*, 1996, **383**, 802-804.
18. M. Pelton, G. Smith, N. F. Scherer and R. A. Marcus, *Proc. Natl. Acad. Sci. USA*, 2007, **104**, 14249-14254.
19. S. Wu, G. Han, D. J. Milliron, S. Aloni, V. Altoe, D. V. Talapin, B. E. Cohen and P. J. Schuck, *Proc. Natl. Acad. Sci. USA*, 2009, **106**, 10917-10921.

20. R. Weissleder, *Nat. Biotechnol.*, 2001, **19**, 316-317.
21. Y. M. Bae, Y. I. Park, S. H. Nam, J. H. Kim, K. Lee, H. M. Kim, B. Yoo, J. S. Choi, K. T. Lee, T. Hyeon and Y. D. Suh, *Biomaterials*, 2012, **33**, 9080-9086.
22. L. Cheng, K. Yang, S. Zhang, M. Shao, S. Lee and Z. Liu, *Nano Res.*, 2010, **3**, 722-732.
23. J. Pichaandi, J.-C. Boyer, K. R. Delaney and F. C. J. M. van Veggel, *J. Phys. Chem. C*, 2011, **115**, 19054-19064.
24. J. Zhou, Z. Liu and F. Li, *Chem. Soc. Rev.*, 2012, **41**, 1323-1349.
25. C. Wang, L. Cheng, H. Xu and Z. Liu, *Biomaterials*, 2012, **33**, 4872-4881.
26. L. Cheng, K. Yang, M. Shao, S.-T. Lee and Z. Liu, *J. Phys. Chem. C*, 2011, **115**, 2686-2692.
27. F. Wang, R. Deng, J. Wang, Q. Wang, Y. Han, H. Zhu, X. Chen and X. Liu, *Nature Mater.*, 2011, **10**, 968-973.
28. Y. Lu, J. Zhao, R. Zhang, Y. Liu, D. Liu, E. M. Goldys, X. Yang, P. Xi, A. Sunna, J. Lu, Y. Shi, R. C. Leif, Y. Huo, J. Shen, J. A. Piper, J. P. Robinson and D. Jin, *Nature Photon.*, 2014, **8**, 32-36.
29. Q. Zhan, J. Qian, H. Liang, G. Somesfalean, D. Wang, S. He, Z. Zhang and S. Andersson-Engels, *ACS Nano*, 2011, **5**, 3744-3757.
30. Y.-F. Wang, G.-Y. Liu, L.-D. Sun, J.-W. Xiao, J.-C. Zhou and C.-H. Yan, *ACS Nano*, 2013, **7**, 7200-7206.
31. H. B. Na and T. Hyeon, *J. Mater. Chem.*, 2009, **19**, 6267-6273.
32. R. Kumar, M. Nyk, T. Y. Ohulchanskyy, C. A. Flask and P. N. Prasad, *Adv. Funct. Mater.*, 2009, **19**, 853-859.
33. J. Zhou, M. Yu, Y. Sun, X. Zhang, X. Zhu, Z. Wu, D. Wu and F. Li, *Biomaterials*, 2011, **32**, 1148-1156.
34. Q. Liu, Y. Sun, C. Li, J. Zhou, C. Li, T. Yang, X. Zhang, T. Yi, D. Wu and F. Li, *ACS Nano*, 2011, **5**, 3146-3157.
35. Y. I. Park, H. M. Kim, J. H. Kim, K. C. Moon, B. Yoo, K. T. Lee, N. Lee, Y. Choi, W. Park, D. Ling, K. Na, W. K. Moon, S. H. Choi, H. S. Park, S.-Y. Yoon, Y. D. Suh, S. H. Lee and T. Hyeon, *Adv. Mater.*, 2012, **24**, 5755-5761.
36. F. Chen, W. Bu, S. Zhang, X. Liu, J. Liu, H. Xing, Q. Xiao, L. Zhou, W. Peng, L. Wang and J. Shi, *Adv. Funct. Mater.*, 2011, **21**, 4285-4294.

37. F. Chen, W. Bu, S. Zhang, J. Liu, W. Fan, L. Zhou, W. Peng and J. Shi, *Adv. Funct. Mater.*, 2013, **23**, 298-307.
38. L. Cheng, K. Yang, Y. Li, J. Chen, C. Wang, M. Shao, S.-T. Lee and Z. Liu, *Angew. Chem. Int. Ed.*, 2011, **50**, 7385-7390.
39. A. Xia, Y. Gao, J. Zhou, C. Li, T. Yang, D. Wu, L. Wu and F. Li, *Biomaterials*, 2011, **32**, 7200-7208.
40. C. Zhong, P. Yang, X. Li, C. Li, D. Wang, S. Gai and J. Lin, *RSC Adv.*, 2012, **2**, 3194-3197.
41. Y. Liu, K. Ai, J. Liu, Q. Yuan, Y. He and L. Lu, *Angew. Chem. Int. Ed.*, 2012, **51**, 1437-1442.
42. M. He, P. Huang, C. Zhang, H. Hu, C. Bao, G. Gao, R. He and D. Cui, *Adv. Funct. Mater.*, 2011, **21**, 4470-4477.
43. X. Zhu, J. Zhou, M. Chen, M. Shi, W. Feng and F. Li, *Biomaterials*, 2012, **33**, 4618-4627.
44. Q. Xiao, W. Bu, Q. Ren, S. Zhang, H. Xing, F. Chen, M. Li, X. Zheng, Y. Hua, L. Zhou, W. Peng, H. Qu, Z. Wang, K. Zhao and J. Shi, *Biomaterials*, 2012, **33**, 7530-7539.
45. Y. Sun, X. Zhu, J. Peng and F. Li, *ACS Nano*, 2013, **7**, 11290-11300.
46. N. M. Idris, M. K. Gnanasammandhan, J. Zhang, P. C. Ho, R. Mahendran and Y. Zhang, *Nat. Med.*, 2012, **18**, 1580-1585.
47. Q. Xiao, X. Zheng, W. Bu, W. Ge, S. Zhang, F. Chen, H. Xing, Q. Ren, W. Fan, K. Zhao, Y. Hua and J. Shi, *J. Am. Chem. Soc.*, 2013, **135**, 13041-13048.
48. Y. Dai, H. Xiao, J. Liu, Q. Yuan, P. Ma, D. Yang, C. Li, Z. Cheng, Z. Hou, P. Yang and J. Lin, *J. Am. Chem. Soc.*, 2013, **135**, 18920-18929.